ACS APPLIED MATERIALS & INTERFACES

Research Article

www.acsami.org

Binder-Free Carbon Nanotube Electrode for Electrochemical Removal of Chromium

Haitao Wang and Chongzheng Na*

Department of Civil and Environmental Engineering and Earth Sciences, University of Notre Dame, Notre Dame, Indiana 46556, United States

Supporting Information

ABSTRACT: Electrochemical treatment of chromium-containing wastewater has the advantage of simultaneously reducing hexavalent chromium (Cr^{VI}) and reversibly adsorbing the trivalent product (Cr^{III}), thereby minimizing the generation of waste for disposal and providing an opportunity for resource reuse. The application of electrochemical treatment of chromium is often limited by the available electrochemical surface area (ESA) of conventional electrodes with flat surfaces. Here, we report the preparation and evaluation of carbon nanotube (CNT) electrodes consisting of vertically aligned CNT arrays directly grown on stainless steel mesh (SSM). We show that the 3-D organization of CNT arrays increases ESA up to 13 times compared to SSM. The increase of ESA is correlated with the length of CNTs, consistent with a mechanism of roughness-induced ESA enhancement. The increase of ESA directly benefits Cr^{VI} reduction by proportionally accelerating reduction without compromising the electrode's ability to adsorb Cr^{III}. Our results suggest that the rational design of electrodes with hierarchical structures represents a feasible approach to improve the performance of electrochemical treatment of contaminated water.

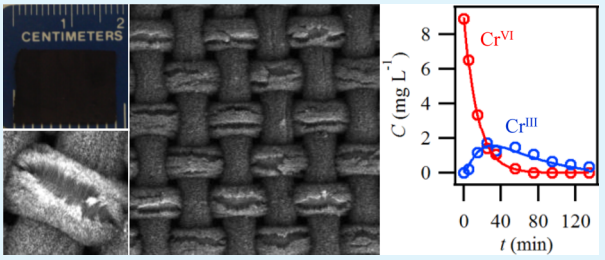

KEYWORDS: *three-dimensional electrode, carbon nanotube array, composite without polymer binder, industrial wastewater, chromium reduction kinetics, chromium electrosorption, Langmuir isotherm*

INTRODUCTION

Chromium (Cr) is widely used in manufacturing dyes and paints, chrome plating, and leather tanning and thus is a major pollutant of the waste streams generated by these industrial processes.[1] Inappropriate disposal of chromium can contaminate the receiving water body, particularly when chromium exists in the hexavalent state (Cr^{VI}) as chromate (CrO_4^{2-}) and dichromate ($Cr_2O_7^{2-}$). Both anions are nonbiodegradable carcinogens[2−4] and highly mobile with surface and ground waters. The discharge of chromium is regulated at least in developed counties (e.g., below 50 $\mu g\ L^{-1}$ in the United States).[5,6]

The decontamination of Cr^{VI}-containing wastewater often involves two steps. First, Cr^{VI} is reduced to trivalent chromium (Cr^{III}) by iron or sulfide:[7−11]

$$CrO_4^{2-} + 8H^+ + 3e^- \rightarrow Cr^{3+} + 4H_2O \quad (1)$$

Second, Cr^{III} is separated from water by precipitation or sorption, taking the advantage of the low solubility of Cr^{III} (also less toxic[12]).[13−15] The two-step treatment is often considered more efficient and economical than single-step separation methods such as adsorption,[16] ion exchange,[17] reverse osmosis,[18] and membrane filtration.[19,20] The disadvantage of the two-step method is the production of a large quantity of sludge and spent adsorbent for disposal.

The electrochemical treatment of Cr^{VI}-contaminated water can reduce Cr^{VI} to Cr^{III} and then separate it from water without producing sludge or spent adsorbent.[21] To do so, the working electrode is negatively polarized to provide electrons for Cr^{VI} reduction and then adsorb Cr^{III} cations through electrostatic attraction. The electrode can be regenerated by reversing the polarization, which releases Cr^{III} for recollection and reuse. The constraint of the electrochemical treatment is the slow kinetics for Cr^{VI} reduction because the negatively polarized electrode repulses Cr^{VI} anions. The kinetics of Cr^{VI} reduction can be substantially improved by increasing the electrochemical surface area (ESA) of the electrode, which represents the area of the electrode's surface that can participate in an electrochemical process. One proposed strategy for increasing ESA is depositing nanomaterials such as carbon nanotubes (CNTs) on a glass carbon electrode.[22−24] To do so, polymer binders such as poly(vinylene fluoride) and Nafion are often required to deposit an adequate amount of nanomaterials.[25−27] The use of binders can, however, lead to structural disintegration under chemical attacks, reduced electrical conductivity, and increased mass-transfer resistance.[27−30]

Here, we report the design and fabrication of a binder-free CNT electrode by growing vertically aligned CNTs ($VACNT_S$) on stainless steel mesh (SSM). Compared to SSM, the growth of VACNTs increases ESA by more than an order of

Received: August 28, 2014
Accepted: November 3, 2014
Published: November 3, 2014

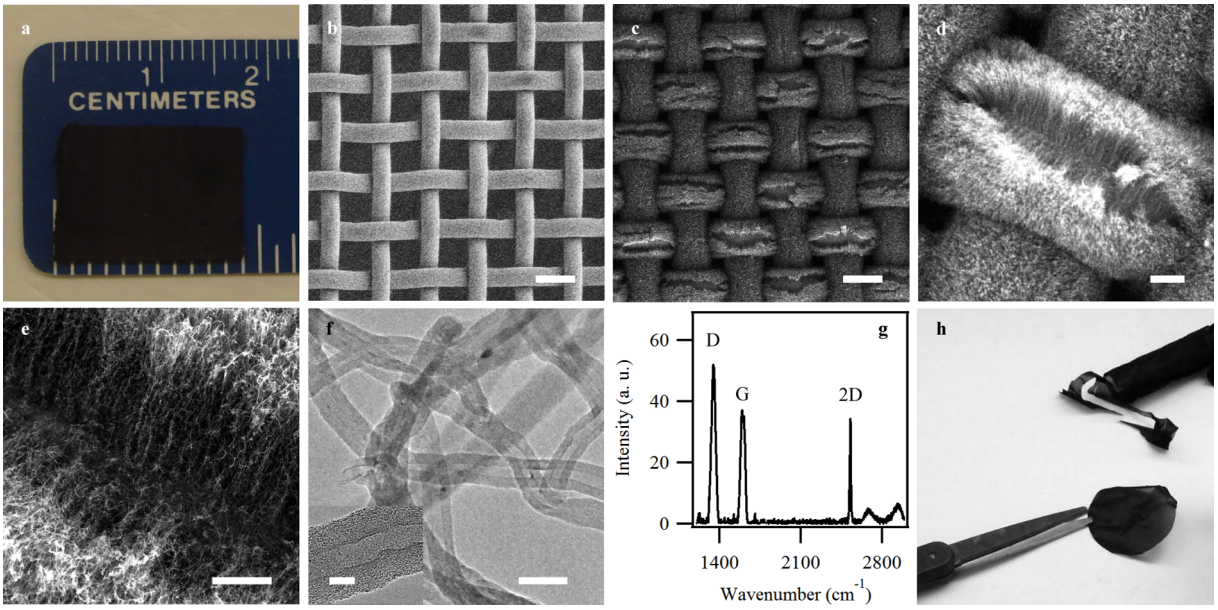

Figure 1. Physical characteristics of a typical CNT electrode. (a) Digital photograph. (b) Scanning electron micrograph (SEM) of bare stainless steel mesh (SSM). (c) SEM of SSM after growing vertically aligned CNT arrays. (d and e) SEMs showing the organization of CNT arrays. (f) Transmission electron micrograph (TEM) of individual CNTs removed from the electrode by sonication; (inset) high-resolution TEM. (g) Raman spectrum. (h) Cutting of the electrode with scissors. Scale bars: (b and c) 50 μm, (d) 10 μm, (e) 5 μm, (f) 40 nm, and (f, inset) 10 nm.

magnitude. We show that the increased ESA can directly benefit Cr^{VI} reduction by proportionally accelerating the reduction rate without compromising the ability to adsorb Cr^{III}.

RESULTS

Carbon Nanotube Electrode. The binder-free CNT electrode was prepared by growing VACNTs directly on SSM after activation using chemical vapor deposition (CVD).[31] A typical CNT electrode is shown in Figure 1. Visually, the electrode resembles a piece of dark cloth (Figure 1a). The electrode is prepared using a piece of 304 SSM with a 400 × 400 openings per square inch (wire diameter, 25 μm; opening size, 38 × 38 μm) as support for VACNTs (Figure 1b). Scanning electron microscopy (SEM) shows that SSM openings are closed up by VACNTs grown vertically on stainless steel wires (Figure 1c). The CNT arrays show cracks in the direction of gas flow, presumably formed under stress. Through the cracks, the vertical alignment of individual CNTs is visible (Figure 1d,e). Transmission electron microscopy (TEM) shows that individual CNTs have a diameter of ca. 30 nm with ca. 30 walls (Figure 1f). Raman spectroscopy confirms that CNTs are of good quality with a D/G ratio of 1.3 (size of in-plane graphene crystallites: 6.4 nm; Figure 1g).[32,33] Between individual CNTs, there are channels of tens of nanometers wide that can facilitate mass transfer in and out of CNT arrays. Because stainless steel wires are thin, the CNT electrode can be readily cut into any arbitrary shape using a pair of scissors (Figure 1h), providing flexibility to device designs. The CNT electrode is found to maintain excellent structural integrity both after being put in contact with solid matters (Figure S1, Supporting Information) and immersed in aqueous solutions (Figure S2, Supporting Information).

Using high-resolution TEM (e.g., Figure 1f), we did not observe any metal particles inside the CNT nanotubes directly grown on SSM. This is different from CNTs prepared by catalyst particles dispersed on powder supports. Because the dispersed catalysts do not have high affinity with the supports and thus are mobile at the elevated temperature of CVD,[34,35] CNTs prepared using powder supports often contain 4−50% (by weight) residual catalysts as particles inside the nanotubes.[36] To eliminate the influence of residual catalysts on the CNTs' reactivity, aggressive treatment with boiling concentrated nitric acid is often required to open up the nanotubes in order to remove the residual catalytic nanoparticles.[37,38] The absence of catalyst nanoparticles inside CNTs directly grown on SSM suggests that our unique synthesis technique has greatly reduced catalyst mobility and thus prevented the contamination of CNTs by residual catalytic nanoparticles.[39,40] As a result, it is not necessary to treat the CNT electrodes for residual catalytic nanoparticles before use.

Electrochemical Surface Area of the CNT Electrode. The arrangement of CNT arrays on SSM represents a 3-D hierarchical structure.[41,42] This structure has a surface area much greater than that of a metal-sheet electrode with the same macroscopic size. However, not all the surfaces of individual CNTs can participate in electrochemical reactions and the portion that does gives ESA. To facilitate discussion, we herein define three terms related to the surface area of an electrode. First, we define the geometric surface area (GSA) as half of a surface area of a two-dimension plate. Second, the specific overall surface area (sOSA) is defined as the ratio of the total surface area of a CNT electrode to the GSA of the SSM supporting it. Third, we define the specific electrochemical surface area (sESA) as the ratio of ESA to GSA. Understanding the relationships of sESA with the kinetics of Cr^{VI} reduction and the capacity of Cr^{III} sorption is the main objective of this study.

The ESA of the CNT electrode was measured by cyclic voltammetry in an aqueous solution containing 5 mM $K_3Fe(CN)_6$ as the redox probe and 0.1 M KNO_3 as the background electrolyte. As shown in Figure 2a, the voltammogram has two distinctive Faradaic peaks over the capacitive background, produced by the reversible reduction of ferricyanide to ferrocyanide:[43,44]

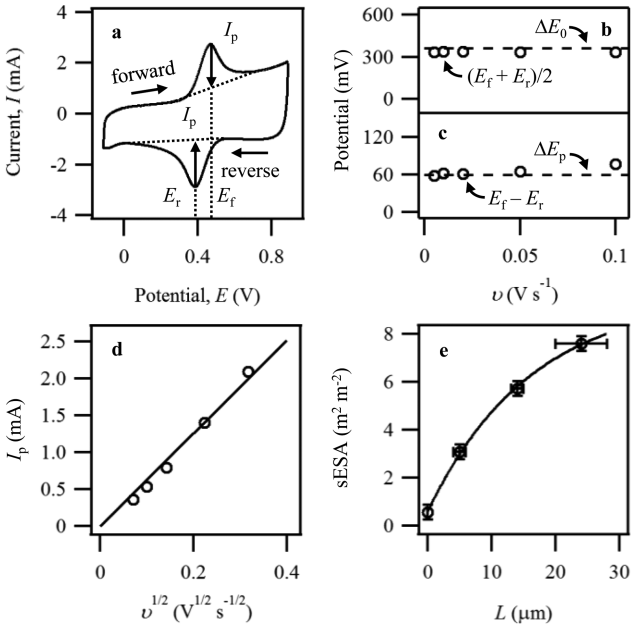

Figure 2. Estimation of electrochemical surface area (ESA) by the cyclic voltammetry of iron cyanide. (a) Typical voltammogram (scan rate: υ = 100 mV s^{-1}). (b) Comparison of $(E_f + E_r)/2$ with the standard potential E_0 of ferricyanide reduction (dashed line: 370 mV). (c) Comparison of $E_f - E_r$ with the theoretical value of ΔE_p = 59 mV (dashed line). (d) Linear correlation between I_p and $\upsilon^{1/2}$. (e) Increase of specific ESA with CNT length L: sESA = 15.1(±0.7) − 14.1(±0.7) exp[−0.063(±0.005)L] (R^2 = 0.999). Solution: 5 mM potassium ferricyanide and 0.1 M potassium nitrate. Electrode: $a - d$, L = 14(±1) μm.

$$[Fe^{III}(CN)_6]^{3-} + e^- \rightleftarrows [Fe^{II}(CN)_6]^{4-} \quad (2)$$

According to the Nernst equation,[45] the summation of the peak potentials should equal to twice the standard potential of reaction 2 (E_0 = 370 mV):[46]

$$(E_f + E_r)/2 = E_0 \quad (3)$$

whereas their difference should have a value of ΔE_p = 59 mV at 25 °C:

$$E_f - E_r = \Delta E_p \quad (4)$$

As shown in Figure 2b,c, $(E_f + E_r)/2$ = 426(±3) mV and $E_f - E_r$ = 65(±7) mV, which satisfy eqs 3 and 4 after considering overpotential (due to concentration difference between the bulk solution and the electrode surface as well as resistance to diffusion through the electrical double layer near the electrode surface),[47,48] indicating that the measurement system is configured properly. ESA is estimated from the mass-transfer controlled behavior of reaction 2 using the Randles-Ševčik equation:[45]

$$I_p = 268600 n^{3/2} \mathrm{ESA} D^{1/2} C_T \upsilon^{1/2} \quad (5)$$

where I_p is the peak current (averaged from forward and reverse scans), n = 1 is the number of electrons transferred in the ferric-to-ferrous reduction, $D = 6.7 \times 10^{-6}$ cm^2 s^{-1} is the diffusion coefficient,[49] $C_T = 5 \times 10^{-6}$ mol cm^{-3} is the total concentration of iron cyanide, and υ is the scan rate. As shown in Figure 2d, linear regression of I_p and $\upsilon^{1/2}$ gives ESA = 1.14(±0.06) cm^2 (R^2 = 0.99).

According to ESA = sESA × GSA and GSA = 0.2 cm^2, sESA = 5.7(±0.3) m^2 m^{-2}, which is approximately 8% of the corresponding sOSA of 68(±0.3) m^2 m^{-2}. To estimate sOSA, the total surface area of the electrode was measured using the Brunauer−Emmett−Teller (BET) adsorption of nitrogen (Figure S3, Supporting Information), which gave a specific surface area of 0.38 m^2 g^{-1} (36.6 m^2 g^{-1} excluding the mass of SSM or 13.8 cm^2 for the electrode with GSA = 0.2 cm^2 and a mass of 3.6 mg). Electrodes with different CNT lengths were prepared by shortening or extending the CVD synthesis time. As the VACNT length L increases from 0 to 24 μm, sESA increases exponentially from 0.57(±0.31) m^2 m^{-2} (bare SSM) to 7.6(±0.3) m^2 m^{-2}, as shown in Figure 2e. This represents a 13× improvement of sESA by VACNT growth.

Electrochemical Reduction of Cr^{VI}. The first step of electrochemical treatment of Cr^{VI}-contaminated water, namely the reduction of Cr^{VI} to Cr^{III}, was achieved by negatively polarizing the CNT cathode. The Cr^{VI}-contaminated water was simulated using an aqueous solution containing $K_2Cr_2O_7$ and Na_2SO_4. In this solution system, the increase of pH by reaction 1 near the cathode can lead to the formation of $Cr(OH)_3$ colloids and eventually the passivation of cathode by polynuclear $Cr(OH)_3Cr(OH)CrO_4$ coating.[50] The presence of sulfate can prevent the formation of colloids and coating by coordinating with Cr^{III} in solution.[51] The use of monovalent K^+ and Na^+ as balancing cations minimizes the competition with Cr^{3+} in electrosorption, where ions with greater ionic charges and smaller hydrated radii are preferably adsorbed. Compared to K^+ and Na^+, Cr^{3+} has a similar hydrated radius (461 pm vs 331 pm for K^+ and 358 pm for Na^+) but a much greater amount of ionic charge; therefore, K^+ and Na^+ will not interfere with the electrosorption of Cr^{3+}.[52]

Figure 3 shows an example obtained using the electrode with GSA = 9 cm^2 and sESA = 5.7(±0.3) m^2 m^{-2}. In a solution containing ca. 9 mg L^{-1} $K_2Cr_2O_7$ and 10 g L^{-1} Na_2SO_4 (100 mL at pH 3), the logarithmic reduction of Cr^{VI} concentration exhibits pseudo first order kinetics when the electrode is polarized at E = −1.4 V (vs the standard hydrogen electrode; Figure 3a):

$$\ln(C/C_0) = -k_1 t \quad (6)$$

where C_0 and C are initial and residual concentrations, t is time, and k_1 is the rate constant. For volume V = 50−200 mL, k_1 is found to correlate inversely with V (Figure 3b), indicating

$$k_1 = k_V \mathrm{GSA}/V \quad (7)$$

The volume normalized pseudo-first-order rate constant (k_V) depends on both E and pH. With the increase of polarization (i.e., E becomes increasingly negative), k_V increases rapidly from zero at E = 0 to 432(±11) L m^{-2} h^{-1} at E = −1.4 V (Figure 3c). Further increase of polarization does not lead to further increase of k_V, suggesting that the kinetics of Cr^{VI} reduction has entered an ESA-controlled regime. As pH increases, k_V decreases rapidly from 606(±15) L m^{-2} h^{-1} at pH = 1 to 135(±10) L m^{-2} h^{-1} at pH = 6 (Figure 3d), consistent with reaction 1 that involves proton as a reactant.

At E = −1.4 V, hydrogen bubbles formed by the reduction of water can be seen evolving near the cathode. This is consistent with the H_2 evolution potential of −0.63 V measured for CNT electrodes in solutions without Cr^{VI} (Figure S4, Supporting Information).[53,54] The reduction of water, which increases with increasing the negative potential on the cathode (cf. Figure S4, Supporting Information), produces highly reactive atomic

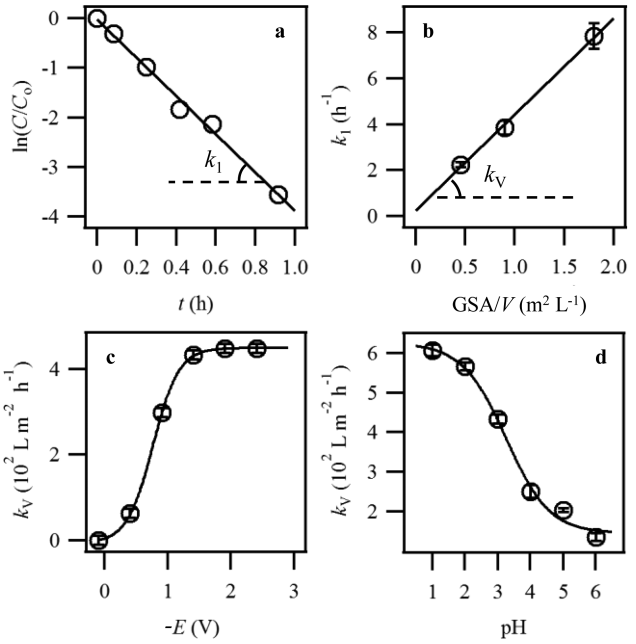

Figure 3. Estimation of (a) pseudo-first-order rate constant for Cr^{VI} reduction, (b) its dependence on reaction volume V, and the dependence of volume normalized pseudo first order rate constant on (c) potential and (d) pH. Solution pH for a, b, and c: 3. Solution volume for a, c, and d: V = 100 mL. Potential for a, b, and d: −1.4 V. Electrode: L = 14(±1) μm.

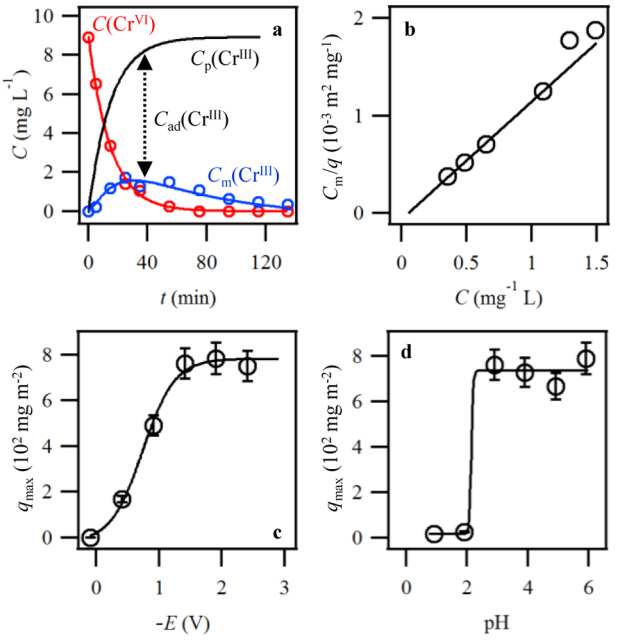

Figure 4. Electrosorption of Cr^{III}: (a) changes of Cr^{IV} and Cr^{III} concentrations with time, (b) conformation to the Langmuir isotherm (pH 3), and dependence on (c) potential and (d) pH. Solution: $K_2Cr_2O_7$, 9 mg L^{-1}; volume, 100 mL. Electrode: L = 14(±1) μm. Potential: E = −1.4 V.

hydrogen radicals that reduce Cr^{VI} indirectly in addition to the direct reduction of Cr^{VI} on the CNT surface.[55] The unreacted hydrogen radicals combine into hydrogen gas. The elucidation of direct and indirect pathways of Cr^{VI} reduction is, however, beyond the scope of this study.

Electrosorption of Cr^{III}. Compared to Cr^{VI}, the concentration of the reduction product Cr^{III} shows a complex time dependence, as illustrated in Figure 4. The Cr^{III} concentration first increases with time, reaches a maximum around t = 30 min, and decreases to nearly zero (Figure 4a). Furthermore, the measured Cr^{III} concentration is much lower than the concentration predicted by the stoichiometry of reaction 1. We attribute the difference between the predicted and measured concentrations (C_p and C_m) to the electrosorption of Cr^{III} cations such as Cr^{3+} and $Cr(OH)^{2+}$ by the negatively polarized electrode:[21]

$$C_{ad}(Cr^{III}) = C_p(Cr^{III}) - C_m(Cr^{III}) \quad (8)$$

where $C_p = C_0(Cr^{VI}) - C(Cr^{VI})$. The electrosorption of Cr^{III} is the second step of Cr removal.

The amount of Cr^{III} adsorbed per unit of GSA is then calculated as

$$q = C_{ad}V/GSA \quad (9)$$

A linear correlation is found between C/q and C_m for t > 30 min, suggesting that the electrosorption of Cr^{III} conforms to the classical Langmuir isotherm (Figure 4b):[56]

$$\frac{C_m}{q} = \frac{C_m}{q_{max}} + \frac{1}{q_{max}K_s} \quad (10)$$

where q_{max} is the maximum sorption capacity, and K_s is the equilibrium constant. The conformation to eq 10 suggests that the electrosorption of Cr^{III} can be considered as an equilibrium-controlled process at least after 30 min. In addition, the linearity has a near zero intercept, consistent with a large value for K_s that favors the partitioning of Cr^{III} cations on the electrode rather than staying in solution.

Comparisons of q_{max} values obtained at different potential and pH conditions show that q_{max} increases with increasing $-E$ and pH, approaching a maximal value of 746(±44) mg m^{-2} for $-E \geq 1.4$ V and pH ≥ 3 (Figure 4c,d). The dependence of q_{max} on $-E$ suggests that electrostatic attraction controls Cr^{III} electrosorption at small polarization, which becomes limited by the availability of Cr^{III} when polarization is sufficiently negative. The dependence of q_{max} on pH suggests that proton competes with Cr^{III} in electrosorption and the competition diminishes as the proton concentration decreases.

Effects of ESA on Cr^{VI} Reduction and Cr^{III} Sorption. Effects of ESA on Cr^{VI} reduction and Cr^{III} sorption are assessed by comparing k_V and q_{max} values obtained using electrodes with different CNT lengths, as shown in Figure 5. k_V is linearly correlated with sESA (Figure 5a):

$$k_V = k_{ESA} \times sESA \quad (11)$$

suggesting the existence of a surface-normalized constant k_{ESA} = 76(±5) L m^{-2} h^{-1} at pH 3. Similar to the ferric-to-ferrous reduction, the reduction of Cr^{VI} to Cr^{III} is rapid at the electrode−solution interface. The overall reduction rate is controlled by the transfer of negatively charged chromate and dichromate anions to the negatively charged electrode. Different from k_V, q_{max} is insensitive to the change of ESA and has an average value of 820(±28) mg m^{-2} (Figure 5b), suggesting that electrosorption is not controlled by ESA and thus not by mass transfer. This is consistent with the mechanism of electrosorption of cations by a negatively polarized electrode, which is controlled by the strength of the electrical field and the presence of competing ions.

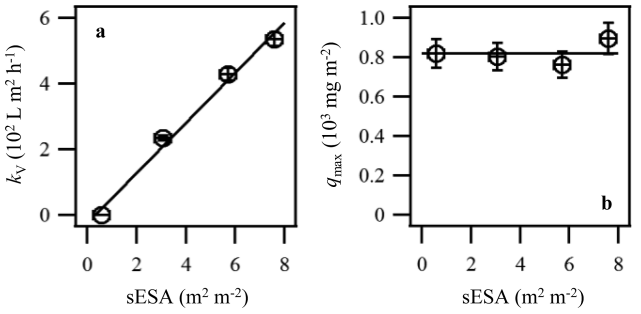

Figure 5. Effects of ESA on Cr^{VI} reduction and Cr^{III} sorption. Dependence of (a) volume normalized pseudo-first-order rate constant (k_V) and (b) maximum sorption capacity q_{max} on specific electrochemical surface area sESA. Solution: $K_2Cr_2O_7$, 9 mg L^{-1}; pH, 3. Potential: E = −1.4 V.

Regeneration of Electrode and Recollection of Cr^{III}. The dependence of q_{max} on pH also suggests that adsorbed Cr^{III} can be readily removed in an acidic solution, providing a method for recycling chromium and regenerate the electrode. The removal process can be further promoted by reversing the potential on the CNT electrode from being negative to being positive. This is demonstrated in Figure 6. First, the

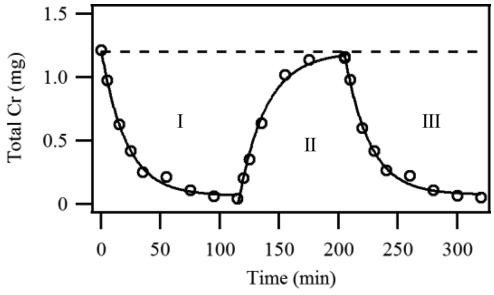

Figure 6. Recollection of adsorbed Cr^{III} and regeneration of the CNT electrode. Solutions: I and III, 100 mL $K_2Cr_2O_7$ at pH 3; II, 30 mL 0.1 M H_2SO_4. Electrode: L = 14(±1) μm. Potential: I and III, −1.4 V; II, 1.0 V.

electrochemical treatment was performed with 100 mL of aqueous solution containing 12 mg L^{-1} Cr^{VI} at pH 3 and operated at E_0 = −1.4 V. After 115 min, 96% of Cr^{VI} was reduced to Cr^{III}, which was in turn adsorbed by the electrode. Second, the electrode was immersed in 30 mL of pH 1 aqueous solution, and the potential on the electrode was reversed to E = 1.0 V. In 90 min, 97% of the adsorbed Cr^{III} desorbed from the electrode, as confirmed by the measurement of Cr^{III} concentration in the recycling solution. Third, the regenerated electrode was used to treat the same Cr^{VI}-containing solution, exhibiting performance similar to that of the new electrode with 96% removal in 115 min.

DISCUSSION

The linear correlation of k_V and sESA suggests that increasing ESA is beneficial to the electrochemical removal of Cr^{VI}, whose kinetics is controlled by Cr^{VI} reduction. The asymptotic relationship between sESA and L suggests that sESA can reach a maximum value of 15.1(±0.7) m^2 m^{-2} with infinitely long CNTs. In synthesis, the CNT length is limited by the longevity of the growth catalysts, which aggregate and coalesce under the high temperature of CVD. We achieved a value of sESA = 7.6(±0.3) m^2 m^{-2} by growing CNTs in CVD for 30 min. This sESA is more than 3 times greater than the values achieved previously for CNT electrodes prepared with both vertically aligned and randomly attached CNTs.[57,58] Further increase of synthesis time is found not to further increase the length of VACNTs. Instead, amorphous carbon is formed due to the deactivation of the Fe/Ni nanoparticles on SSM.

We propose that at least two geometric factors have contributed to the increase of sESA as L increases, including (1) filling of the void spaces left by the SSM openings and (2) creation of curved surfaces. SSM has an sESA of 0.6(±0.3) m^2 m^{-2}, consistent with the specific cross-section area of SSM: $[(25 + 38)^2 - 38^2]/(25 + 38)^2 = 0.635$ m^2 m^{-2}. Both values are smaller than the specific surface area of a plate electrode (sESA = 1 m^2 m^{-2}). Growing CNTs fills up the void space and thus improves sESA to unity.

Further increase of sESA from 1 to 7.6(±0.3) m^2 m^{-2} is attributed to the curvature of individual CNTs and the filling of the space between them. The curvature effect is illustrated in Figure 7. A square plate electrode with a flat surface intersects

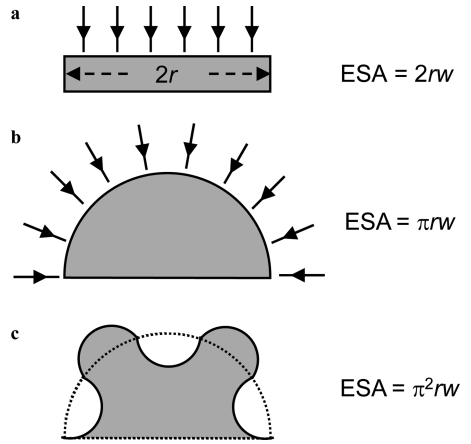

Figure 7. Increasing electrochemical surface area (ESA) by increasing electrode surface roughness. (a) Plate electrode. (b) Half-sphere electrode. (c) Half-sphere electrode with surface being further divided by smaller half spheres.

with the electrical field lines normally (Figure 7a). This gives an ESA equivalent to its geometrical surface area defined by length 2r and width w of the plate: 2rw. Replacing the plate with a half cylinder having radius r increases the area of the receiving surface. To intersect normally with the curved receiving surface, field lines are bent near the electrode surface (Figure 7b). This increases ESA to πrw while maintaining the same GSA (note: by definition, GSA is always associated with the plate geometry), giving sESA = π/2. The surface of the half cylinder can be further divided by smaller half cylinders (Figure 7c), which further increases sESA to π^2/2. Repeating this operation for n times, we have sESA = π^n/2. To obtain a 7.6-times increase of sESA, a value of n = 2.4 is sufficient. This analysis is consistent with the understanding that increasing the roughness of an electrode surface increases sESA.[59]

Growing VACNTs adds roughness to the otherwise flat SSM surface. The roughness originates from both the large number of CNTs and the curvature of individual CNTs (Figure 1e). Because individual CNTs are spaced from each other, contributions to roughness and thus sESA come from not only the very top portion of CNTs but also a large portion in the middle of the nanotubes. As a result, longer CNTs

contribute more to sESA although the curvature of CNTs and the porosity of CNT arrays remain constant regardless of CNT length (Figure S3, Supporting Information). This is equivalent to state that sESA increases proportionally with the increase of CNT mass fraction, as supported by our measurements (Figure S5, Supporting Information). As CNTs grow longer, however, the area between individual CNTs that is projected to receive the electrical field lines begins to fill up, leading to a limiting sESA as we have observed.

The large sESA makes CNT electrodes particularly advantageous for removing recalcitrant contaminants such as Cr^{VI}. With $L = 24\ \mu m$ and sESA = 7.6 $m^2\ m^{-2}$, $k_V = 810\ L\ m^{-2}\ h^{-1}$ at pH 1, which is more than 4 times faster than using the polypyrrole-coated carbon electrode.[60,61] At pH 4, k_V is 250 L $m^{-2}\ h^{-1}$, which is approximately an order of magnitude greater than using an SSM electrode randomly coated with single-walled CNTs.[21]

CONCLUSION

We have prepared carbon nanotube electrodes by growing vertically aligned CNT arrays directly on stainless steel mesh. Compared to randomly orientated CNTs, VACNTs provides a high grafting density with a high degree of roughness and good electrical contact. We show that compared to SSM, growing VACNTs can increase ESA by more than an order of magnitude. The increased ESA can directly benefit Cr^{VI} reduction by proportionally accelerating the reduction reaction without compromising the ability for CNTs to adsorb Cr^{III}. The overall efficiency of chromium removal can be maximized by operating near pH 3 and at $E = -1.4$ V. Furthermore, the adsorbed Cr^{III} can be readily recollected by acid wash, which also regenerates the electrode.

METHODS

All chemicals were of analytical grade, purchased from Sigma-Aldrich and used as received without further purification. Deionized (DI) water (18.2 MΩ cm^{-1}) was generated on site using a Millipore ultrapure water system. The AISI 304 SSM with a mesh size of 400 × 400 openings per square inch was purchased from Grainger (Lake Forest, IL).

Fabrication of Carbon Nanotube Electrode. A piece of 5 × 5 cm^2 SSM was cleaned by sonication in acetone for 15 min and then dried by blowing pure nitrogen gas. The cleaned mesh was rolled and inserted into a 1 in. quartz tubing housed in a horizontal furnace. The furnace was heated to 500 °C in 15 min and held at that temperature for another 15 min to break the chromium-oxide passivation layer and generate iron and nickel catalytic nanoparticles. The temperature was then ramped to 700 °C in 5 min under the flow of 300 sccm argon. Once the temperature was stabilized, 20 sccm acetylene and 150 sccm hydrogen were introduced into the quartz tubing to initiate CNT growth. After 10−30 min, the furnace was cooled to the ambient temperature under the protection of argon before the sample was removed from the quartz tubing.

Characterization of Carbon Nanotube Electrode. Physical properties of SSM and CNT electrodes were characterized using scanning electron microscopy (FEI Magellan 400), transmission electron microscopy (FEI Titan 80−300), Raman spectroscopy (Renishaw 1000), and the BET surface area analysis (Micromeritics ASAP 2000). Because the specific surface areas of CNT electrodes are too small for direct measurements with the BET analyzer, CNT arrays were scratched off SSM using a razor blade. The ESA of the electrode was measured using a three-electrode potentiostat (CHI 610D) and a testing solution of ferric cyanide at room temperature. A piece of SSM or CNT electrode (1 × 0.2 cm), a platinum sheet of the same size, and the Ag/AgCl electrode were used as the working, counter, and reference electrodes, respectively. The solution contained 5 mM potassium ferricyanide and 0.1 M potassium nitrate.

Electrochemical Removal and Recollection of Chromium. Experiments were conducted in the batch mode using the potentiostat. The cathode was either a CNT or SSM electrode (3 × 3 cm), a piece of carbon paper (Fuel Cell Earth LLC, Stoneham, MA) of the same size as the anode, and the Ag/AgCl electrode as reference. The carbon paper was used, instead of a platinum electrode, to prevent the oxidation of Cr^{III} back to Cr^{VI}.[62,63] The carbon paper did not adsorb Cr^{VI} (Figure S6, Supporting Information), likely due to the large size of its anions and the lack of functional groups on the paper's surface. The cathode and anode were separated by a 3 cm gap. A potential (with respect to the standard hydrogen electrode) was applied between the cathode and the reference electrode while the current generated by this potential passes through the anode, forming a three-electrode system.

The experiments were performed with 100 mL $K_2Cr_2O_7$ aqueous solution containing 10 g L^{-1} Na_2SO_4 as the supporting electrolyte. The solution pH was adjusted using concentrated NaOH or H_2SO_4 solutions and confirmed with a pH meter (Fisher Scientific). During experiments, the solution was stirred constantly with a magnetic stirrer to maintain homogeneity. After potential was applied between cathode and anode to initiate reaction, 0.2 mL solution was withdrawn periodically for measurement. Half of the solution was mixed with diphenylcarbazide, which reacted with Cr^{VI} to produce a strong pink color.[64] The intensity of the color was measured using a UV/vis spectrophotometer (Agilent Cary 300), which gave the Cr^{VI} concentration through Beer's law. To determine the concentration of Cr^{III}, the other half of the sample was oxidized with an excess amount of potassium permanganate ($KMnO_4$) to convert Cr^{III} to Cr^{VI}. The concentration of Cr^{VI} was again determined colorimetrically. The Cr^{III} concentration was computed by subtracting the first Cr^{VI} concentration from the second Cr^{VI} concentration.

To study the effects of solution volume, solution chemistry, and electrode surface area on Cr^{VI} reduction and Cr^{III} adsorption, we varied the corresponding experimental condition while keeping other conditions constant. For example, to investigate the volume effect, we fixed the $K_2Cr_2O_7$ concentration, the Na_2SO_4 concentration, and pH at 10 mg L^{-1}, 10 g L^{-1}, and 3 while the solution volume was varied from 50 to 200 mL.

The recollection of Cr^{III} adsorbed by CNTs was performed in 0.1 M sulfuric acid. The Cr^{III} concentration in the recollection solution was determined colorimetrically after the solution being completely oxidized by $KMnO_4$. The amount of recollected Cr^{III} was then computed by multiplying the Cr^{III} concentration with the volume of H_2SO_4 solution used to perform recollection.

ASSOCIATED CONTENT

Supporting Information

Scanning electron micrographs of a CNT electrode before and after being dropped from different heights to ground; optical micrographs of a CNT electrode immersed in solutions having pH from 0 to 7 for 10 and 120 min; specific surface area of CNT arrays on CNT electrodes; linear sweep voltammograms of CNT electrodes for water reduction; correlation of the specific electrochemical surface area of CNT electrodes and their CNT mass fraction; and energy dispersive X-ray spectrum of the carbon-paper anode after being used in the electrochemical treatment of chromium. This material is available free of charge via the Internet at http://pubs.acs.org.

AUTHOR INFORMATION

Corresponding Author

*E-mail: chongzheng.na@gmail.com.

Notes

The authors declare no competing financial interest.

■ ACKNOWLEDGMENTS

We are thankful for financial support from the U.S. Department of Energy Office of Nuclear Energy's Nuclear Energy University Programs, the U.S. National Science Foundation's Environmental Engineering Program, and the University of Notre Dame Sustainable Energy Initiative.

■ REFERENCES

(1) Barnhart, J. Occurrences, Uses, and Properties of Chromium. *Regul. Toxicol. Pharmacol.* **1997**, *26*, S3−S7.
(2) Baruthio, F. Toxic Effects of Chromium and Its Compounds. *Biol. Trace Elem. Res.* **1992**, *32*, 145−153.
(3) Costa, M.; Klein, C. B. Toxicity and Carcinogenicity of Chromium Compounds in Humans. *Crit. Rev. Toxicol.* **2006**, *36*, 155−163.
(4) Katz, S. A.; Salem, H. The Toxicology of Chromium with Respect to Its Chemical Speciation: A Review. *J. Appl. Toxicol.* **1993**, *13*, 217−224.
(5) *Chromium in Drinking-Water: Background Document for Preparation of WHO Guidelines for Drinking-Water Quality*; World Health Organization: Geneva, Switzerland, 2003.
(6) Baral, A.; Engelken, R. D. Chromium-Based Regulations and Greening in Metal Finishing Industries in the USA. *Environ. Sci. Policy* **2002**, *5*, 121−133.
(7) Qin, G.; McGuire, M. J.; Blute, N. K.; Seidel, C.; Fong, L. Hexavalent Chromium Removal by Reduction with Ferrous Sulfate, Coagulation, and Filtration: A Pilot-Scale Study. *Environ. Sci. Technol.* **2005**, *39*, 6321−6327.
(8) Barrera-Díaz, C. E.; Lugo-Lugo, V.; Bilyeu, B. A Review of Chemical, Electrochemical, and Biological Methods for Aqueous Cr(VI) Reduction. *J. Hazard. Mater.* **2012**, *223−224*, 1−12.
(9) Buerge, I. J.; Hug, S. J. Influence of Mineral Surfaces on Chromium(VI) Reduction by Iron(II). *Environ. Sci. Technol.* **1999**, *33*, 4285−4291.
(10) Gould, J. P. The Kinetics of Hexavalent Chromium Reduction by Metallic Iron. *Water Res.* **1982**, *16*, 871−877.
(11) Pettine, M.; Millero, F. J.; Passino, R. Reduction of Chromium(VI) with Hydrogen Sulfide in NaCl Media. *Mar. Chem.* **1994**, *46*, 335−344.
(12) Vincent, J. B. Elucidating a Biological Role for Chromium at a Molecular Level. *Acc. Chem. Res.* **2000**, *33*, 503−510.
(13) Hu, C.-Y.; Lo, S.-L.; Liou, Y.-H.; Hsu, Y.-W.; Shih, K.; Lin, C.-J. Hexavalent Chromium Removal from Near Natural Water by Copper-Iron Bimetallic Particles. *Water Res.* **2010**, *44*, 3101−3108.
(14) Guo, J.; Li, Y.; Dai, R.; Lan, Y. Rapid Reduction of Cr(VI) Coupling with Efficient Removal of Total Chromium in the Coexistence of Zn(0) and Silica Gel. *J. Hazard. Mater.* **2012**, *243*, 265−271.
(15) Zaitseva, N.; Zaitsev, V.; Walcarius, A. Chromium(VI) Removal via Reduction−Sorption on Bi-Functional Silica Adsorbents. *J. Hazard. Mater.* **2013**, *250−251*, 454−461.
(16) Gupta, V. K.; Gupta, M.; Sharma, S. Process Development for the Removal of Lead and Chromium from Aqueous Solutions Using Red Mud—An Aluminium Industry Waste. *Water Res.* **2001**, *35*, 1125−1134.
(17) Dąbrowski, A.; Hubicki, Z.; Podkościelny, P.; Robens, E. Selective Removal of the Heavy Metal Ions from Waters and Industrial Wastewaters by Ion-Exchange Method. *Chemosphere* **2004**, *56*, 91−106.
(18) Ozaki, H.; Sharma, K.; Saktaywin, W. Performance of an Ultra-Low-Pressure Reverse Osmosis Membrane (ULPROM) for Separating Heavy Metal: Effects of Interference Parameters. *Desalination* **2002**, *144*, 287−294.
(19) Wang, K. Y.; Chung, T.-S. Fabrication of Polybenzimidazole (PBI) Nanofiltration Hollow Fiber Membranes for Removal of Chromate. *J. Membr. Sci.* **2006**, *281*, 307−315.
(20) Shukla, A.; Kumar, A. Separation of Cr(VI) by Zeolite-Clay Composite Membranes Modified by Reaction with NO_x. *Sep. Purif. Technol.* **2007**, *52*, 423−429.
(21) Liu, Y.-X.; Yuan, D.-X.; Yan, J.-M.; Li, Q.-L.; Ouyang, T. Electrochemical Removal of Chromium from Aqueous Solutions Using Electrodes of Stainless Steel Nets Coated with Single Wall Carbon Nanotubes. *J. Hazard. Mater.* **2011**, *186*, 473−480.
(22) Wang, S.; Wang, X.; Jiang, S. P. PtRu Nanoparticles Supported on 1-Aminopyrene-Functionalized Multiwalled Carbon Nanotubes and Their Electrocatalytic Activity for Methanol Oxidation. *Langmuir* **2008**, *24*, 10505−10512.
(23) Cheng, Y.; Liu, C.; Cheng, H.-M.; Jiang, S. P. One-Pot Synthesis of Metal−Carbon Nanotubes Network Hybrids as Highly Efficient Catalysts for Oxygen Evolution Reaction of Water Splitting. *ACS Appl. Mater. Interfaces* **2014**, *6*, 10089−10098.
(24) Kongkanand, A.; Vinodgopal, K.; Kuwabata, S.; Kamat, P. V. Highly Dispersed Pt Catalysts on Single-Walled Carbon Nanotubes and Their Role in Methanol Oxidation. *J. Phys. Chem. B* **2006**, *110*, 16185−16188.
(25) Zhao, A.; Masa, J.; Xia, W.; Maljusch, A.; Willinger, M.-G.; Clavel, G.; Xie, K.; Schlögl, R.; Schuhmann, W.; Muhler, M. Spinel Mn-Co Oxide in N-Doped Carbon Nanotubes as a Bifunctional Electrocatalyst Synthesized by Oxidative Cutting. *J. Am. Chem. Soc.* **2014**, *136*, 7551−7554.
(26) Liang, Y.; Wang, H.; Diao, P.; Chang, W.; Hong, G.; Li, Y.; Gong, M.; Xie, L.; Zhou, J.; Wang, J.; Regier, T. Z.; Wei, F.; Dai, H. Oxygen Reduction Electrocatalyst Based on Strongly Coupled Cobalt Oxide Nanocrystals and Carbon Nanotubes. *J. Am. Chem. Soc.* **2012**, *134*, 15849−15857.
(27) Park, B.-H.; Choi, J.-H. Improvement in the Capacitance of a Carbon Electrode Prepared Using Water-Soluble Polymer Binder for a Capacitive Deionization Application. *Electrochim. Acta* **2010**, *55*, 2888−2893.
(28) Hou, C.-H.; Huang, J.-F.; Lin, H.-R.; Wang, B.-Y. Preparation of Activated Carbon Sheet Electrode Assisted Electrosorption Process. *J. Taiwan Inst. Chem. Eng.* **2012**, *43*, 473−479.
(29) Omosebi, A.; Gao, X.; Landon, J.; Liu, K. Asymmetric Electrode Configuration for Enhanced Membrane Capacitive Deionization. *ACS Appl. Mater. Interfaces* **2014**, *6*, 12640−12649.
(30) Porada, S.; Weinstein, L.; Dash, R.; van der Wal, A.; Bryjak, M.; Gogotsi, Y.; Biesheuvel, P. M. Water Desalination Using Capacitive Deionization with Microporous Carbon Electrodes. *ACS Appl. Mater. Interfaces* **2012**, *4*, 1194−1199.
(31) Wang, H.; Dong, Z.; Na, C. Hierarchical Carbon Nanotube Membrane-Supported Gold Nanoparticles for Rapid Catalytic Reduction of *p*-Nitrophenol. *ACS Sustainable Chem. Eng.* **2013**, *1*, 746−752.
(32) Vix-Guterl, C.; Couzi, M.; Dentzer, J.; Trinquecoste, M.; Delhaes, P. Surface Characterizations of Carbon Multiwall Nanotubes: Comparison between Surface Active Sites and Raman Spectroscopy. *J. Phys. Chem. B* **2004**, *108*, 19361−19367.
(33) Delhaes, P.; Couzi, M.; Trinquecoste, M.; Dentzer, J.; Hamidou, H.; Vix-Guterl, C. A Comparison between Raman Spectroscopy and Surface Characterizations of Multiwall Carbon Nanotubes. *Carbon* **2006**, *44*, 3005−3013.
(34) Magrez, A.; Seo, J. W.; Mikó, C.; Hernádi, K.; Forró, L. Growth of Carbon Nanotubes with Alkaline Earth Carbonate as Support. *J. Phys. Chem. B* **2005**, *109*, 10087−10091.
(35) Liu, Q.; Chen, Z.-G.; Liu, B.; Ren, W.; Li, F.; Cong, H.; Cheng, H.-M. Synthesis of Different Magnetic Carbon Nanostructures by the Pyrolysis of Ferrocene at Different Sublimation Temperatures. *Carbon* **2008**, *46*, 1892−1902.
(36) Jansen, R.; Wallis, P. Manufacturing, Characterization and Use of Single Walled Carbon Nanotubes. *Mater. Matters* **2009**, *4*, 23−25.
(37) Pełech, I.; Narkiewicz, U.; Kaczmarek, A.; Jędrzejewska, A.; Pełech, R. Removal of Metal Particles from Carbon Nanotubes Using Conventional and Microwave Methods. *Sep. Purif. Technol.* **2014**, *136*, 105−110.

(38) Niyogi, S.; Hamon, M. A.; Hu, H.; Zhao, B.; Bhowmik, P.; Sen, R.; Itkis, M. E.; Haddon, R. C. Chemistry of Single-Walled Carbon Nanotubes. *Acc. Chem. Res.* **2002**, *35*, 1105−1113.
(39) Wang, H.; Na, C. Synthesis of Millimeter-Long Vertically Aligned Carbon Nanotube Arrays on Aluminum Oxide Buffer Prepared by Layer-by-Layer Assembly of Boehmite Nanoplates. *Carbon* **2014**, *66*, 727−729.
(40) Chen, P.; Chew, L. M.; Xia, W. The Influence of the Residual Growth Catalyst in Functionalized Carbon Nanotubes on Supported Pt Nanoparticles Applied in Selective Olefin Hydrogenation. *J. Catal.* **2013**, *307*, 84−93.
(41) Sun, X.; Chen, T.; Yang, Z.; Peng, H. The Alignment of Carbon Nanotubes: An Effective Route To Extend Their Excellent Properties to Macroscopic Scale. *Acc. Chem. Res.* **2012**, *46*, 539−549.
(42) Meng, F.; Morin, S. A.; Forticaux, A.; Jin, S. Screw Dislocation Driven Growth of Nanomaterials. *Acc. Chem. Res.* **2013**, *46*, 1616−1626.
(43) Van Benschoten, J. J.; Lewis, J. Y.; Heineman, W. R.; Roston, D. A.; Kissinger, P. T. Cyclic Voltammetry Experiment. *J. Chem. Educ.* **1983**, *60*, 702−706.
(44) Daum, P. H.; Enke, C. G. Electrochemical Kinetics of the Ferri-Ferrocyanide Couple on Platinum. *Anal. Chem.* **1969**, *41*, 653−656.
(45) Oldham, K. B.; Myland, J. C.; Bond, A. M. *Electrochemical Science and Technology: Fundamentals and Applications*. John Wiley & Sons, Ltd.: Toronto, Canada, 2012.
(46) Rock, P. A. The Standard Oxidation Potential of the Ferrocyanide-Ferricyanide Electrode at 25 °C and the Entropy of Ferrocyanide Ion. *J. Phys. Chem.* **1966**, *70*, 576−580.
(47) Rubin, H.; Collins, F. C. Concentration Overpotential at Reversible Electrodes. *J. Phys. Chem.* **1954**, *58*, 958−962.
(48) Angell, D. H.; Dickinson, T. The Kinetics of the Ferrous/Ferric and Ferro/Ferricyanide Reactions at Platinum and Gold Electrodes: Part I. Kinetics at Bare-Metal Surfaces. *J. Electroanal. Chem. Interfacial Electrochem.* **1972**, *35*, 55−72.
(49) Yue, R.; Ren, F.; Wang, C.; Xu, J.; Du, Y. Facile Preparation of Flower-Like Graphene-Nanosheet Clusters with the Assistance of Copper Particles and Their Application in Supercapacitors. *RSC Adv.* **2014**, *4*, 500−504.
(50) Levitan, J. Formation of Polynuclear Species during the Electroreduction of Chromic Acid. *J. Electrochem. Soc.* **1964**, *111*, 286−289.
(51) Schlesinger, M.; Paunovic, M. *Modern Electroplating*. 5th ed.; John Wiley & Sons: Hoboken, NJ, 2011.
(52) Hou, C.-H.; Huang, C.-Y. A Comparative Study of Electrosorption Selectivity of Ions by Activated Carbon Electrodes in Capacitive Deionization. *Desalination* **2013**, *314*, 124−129.
(53) Cui, W.; Liu, Q.; Cheng, N.; Asiri, A. M.; Sun, X. Activated Carbon Nanotubes: A Highly-Active Metal-Free Electrocatalyst for Hydrogen Evolution Reaction. *Chem. Commun.* **2014**, *50*, 9340−9342.
(54) Deng, J.; Ren, P.; Deng, D.; Yu, L.; Yang, F.; Bao, X. Highly Active and Durable Non-Precious-Metal Catalysts Encapsulated in Carbon Nanotubes for Hydrogen Evolution Reaction. *Energy Environ. Sci.* **2014**, *7*, 1919−1923.
(55) Hou, Y.; Liu, H.; Zhao, X.; Qu, J.; Chen, J. P. Combination of Electroreduction with Biosorption for Enhancement for Removal of Hexavalent Chromium. *J. Colloid Interface Sci.* **2012**, *385*, 147−153.
(56) Wang, H.; Lin, K.-Y.; Jing, B.; Krylova, G.; Sigmon, G. E.; McGinn, P.; Zhu, Y.; Na, C. Removal of Oil Droplets from Contaminated Water Using Magnetic Carbon Nanotubes. *Water Res.* **2013**, *47*, 4198−4205.
(57) Kim, B.; Chung, H.; Chu, K. S.; Yoon, H. G.; Lee, C. J.; Kim, W. Synthesis of Vertically-Aligned Carbon Nanotubes on Stainless Steel by Water-Assisted Chemical Vapor Deposition and Characterization of Their Electrochemical Properties. *Synth. Met.* **2010**, *160*, 584−587.
(58) Yun, Y.; Gollapudi, R.; Shanov, V.; Schulz, M. J.; Dong, Z.; Jazieh, A.; Heineman, W. R.; Halsall, H. B.; Wong, D. K.; Bange, A. Carbon Nanotubes Grown on Stainless Steel to Form Plate and Probe Electrodes for Chemical/Biological Sensing. *J. Nanosci. Nanotechnol.* **2007**, *7*, 891−897.
(59) Jia, F.; Yu, C.; Deng, K.; Zhang, L. Nanoporous Metal (Cu, Ag, Au) Films with High Surface Area: General Fabrication and Preliminary Electrochemical Performance. *J. Phys. Chem. C* **2007**, *111*, 8424−8431.
(60) Conroy, K. G.; Breslin, C. B. Reduction of Hexavalent Chromium at a Polypyrrole-Coated Aluminium Electrode: Synergistic Interactions. *J. Appl. Electrochem.* **2004**, *34*, 191−195.
(61) Rodríguez, F. J.; Gutiérrez, S.; Ibanez, J. G.; Bravo, J. L.; Batina, N. The Efficiency of Toxic Chromate Reduction by a Conducting Polymer (Polypyrrole): Influence of Electropolymerization Conditions. *Environ. Sci. Technol.* **2000**, *34*, 2018−2023.
(62) El-Sharif, M. R.; McDougall, J.; Chisholm, C. U. Electrodeposition of Thick Chromium Coatings from an Environmentally Acceptable Chromium (III)-Glycine Complex. *Trans. Inst. Met. Finish.* **1999**, *77*, 139−144.
(63) Elsayed, E. M.; Saba, A. E. The Electrochemical Treatment of Toxic Hexavalent Chromium from Industrial Effluents using Rotating Cylinder Electrode Cell. *Int. J. Electrochem. Sci.* **2009**, *4*, 627−639.
(64) Clesseri, L. S.; Greenberg, A. E.; Eaton, A. D. *Standard Methods for the Examination of Water and Wastewater*. American Public Health Association, American Water Works Association, and Water Pollution Control Federation: Washington, DC, 1998.